NASA TECHNICAL NOTE

NASA TN D-7346

NASA TN D-7346

TRANSONIC SINGLE-MODE FLUTTER AND BUFFET OF A LOW ASPECT RATIO WING HAVING A SUBSONIC AIRFOIL SHAPE

by Larry L. Erickson

Ames Research Center
Moffett Field, Calif. 94035

NATIONAL AERONAUTICS AND SPACE ADMINISTRATION • WASHINGTON, D. C. • JANUARY 1974

1. Report No.	2. Government Accession No.	3. Recipient's Catalog No.
NASA TN D-7346		

4. Title and Subtitle	5. Report Date
TRANSONIC SINGLE–MODE FLUTTER AND BUFFET OF A LOW ASPECT RATIO WING HAVING A SUBSONIC AIRFOIL SHAPE	January 1974
	6. Performing Organization Code

7. Author(s)	8. Performing Organization Report No.
Larry L. Erickson	A-4966
	10. Work Unit No.
9. Performing Organization Name and Address	502-32-04
NASA Ames Research Center Moffett Field, Calif. 94035	11. Contract or Grant No.
	13. Type of Report and Period Covered
12. Sponsoring Agency Name and Address	Technical Note
National Aeronautics and Space Administration Washington, D. C. 20546	14. Sponsoring Agency Code

15. Supplementary Notes

16. Abstract

Transonic flutter and buffet results obtained from wind-tunnel tests of a low aspect ratio semispan wing model are presented. The tests were conducted to investigate potential transonic aeroelastic problems of vehicles having subsonic airfoil sections (e.g., the space shuttle). The model employed NACA 00XX-64 airfoil sections in the streamwise direction and had a 14° leading edge sweep angle. Aspect ratio, taper ratio, and average thickness were 4.0, 0.35, and 8 percent, respectively. The model was tested at Mach numbers from 0.6 to 0.95 at angles of attack from 0° to 15°.

Two zero lift flutter conditions were found that involved essentially single normal mode vibrations. With boundary layer trips on the model, flutter occurred in a narrow Mach number range centered at about Mach 0.90. The frequency and motion of this flutter were like that of the first normal mode vibration. With the trips removed flutter occurred at a slightly higher Mach number but in a mode strongly resembling that of the second normal mode.

Several instances of low torsional damping were observed at high angles of attack, but stall flutter was not encountered, except possibly at $M = 0.90, \alpha \approx 13°$. Maximum buffet loads occurred at angles of attack between 10° and 14°. Quantitative results for the maximum wing root bending moments due to buffet are presented in a form suitable for scaling.

17. Key Words (Suggested by Author(s))	18. Distribution Statement
Flutter Buffet Transonic unsteady flow Single degree of freedom Shock stall	Unclassified – Unlimited

19. Security Classif. (of this report)	20. Security Classif. (of this page)	21. No. of Pages	22. Price*
Unclassified	Unclassified	23	Domestic, $2.75 Foreign, $5.25

* For sale by the National Technical Information Service, Springfield, Virginia 22151

SYMBOLS

a	speed of sound, m/sec (in./sec)
$AR = \frac{(2L)^2}{S}$	aspect ratio
b	semichord of wing at $\bar{y} = 0.75$, m (in.)
c	chord length, m (in.)
E	Young's modulus, N/m^2 ($lbf/in.^2$)
EI	wing bending stiffness, $N\text{-}m^2$ ($lbf\text{-}in.^2$)
f	frequency, Hz
G	shear modulus, N/m^2 ($lbf/in.^2$)
GK	wing torsional stiffness, $N\text{-}m^2$ ($lbf\text{-}in.^2$)
$k_1 = \frac{b\omega_1}{V_\infty}$	reduced frequency of first normal mode
ℓ	distance from $\bar{y} = 0.255$ to $\bar{y} = 1.0$ (from end of tongue to wing tip), m (in.)
L	semispan, m (in.)
m_w	wing mass per unit length, kg/m (slugs/ft)
M_∞	free-stream Mach number
M_{cr}	critical Mach number
M_{sep}	free-stream Mach number corresponding to the onset of shock-induced trailing edge separation
$\overline{M}_{dyn}, \overline{M}_{static}$	dynamic and static wing bending moments, respectively, m-N (in.-lb)
p_t	tunnel total (stagnation) pressure, N/m^2 (in.-Hg.)
q_∞	free-stream dynamic pressure, N/m^2 ($lbf/in.^2$)
S	full span wing area, m^2 ($in.^2$)
$\frac{t}{c}$	wing thickness to chord ratio at point of maximum thickness (i.e., at 40 percent chord)

V_∞	free-stream velocity, m/sec (in./sec)
x,y	wing planform coordinates, m (in.)
$\bar{y} = \frac{y}{L}$	
α	angle of attack, deg
ζ_a,ζ_s	aerodynamic and structural damping ratios, respectively, as fraction of critical damping
$\zeta_{1B}(\zeta_{2T})$	net damping ratio ($\zeta_a + \zeta_s$) for mode 1 (2) obtained from bending (torsion) gage signal
μ	mass ratio, $\frac{\int m_w\, dy}{\rho_\infty \frac{\pi}{4} \int c^2\, dy}$
ν	Poisson's ratio
ρ_∞	free-stream air density, kg/m^3 (slugs/ft^3)
σ_B,σ_T	standard deviation of bending and torsion gage signals, respectively
ω_1,ω_2	first and second normal mode model frequencies, respectively, rad/sec
ω_h,ω_θ	uncoupled normal mode frequencies in translation and rotation, respectively, rad/sec

Subscript

o	value at end of support tongue (i.e., at $\bar{y} = 0.255$)

TRANSONIC SINGLE–MODE FLUTTER AND BUFFET OF A LOW ASPECT RATIO WING HAVING A SUBSONIC AIRFOIL SHAPE

Larry L. Erickson

Ames Research Center

SUMMARY

Transonic flutter and buffet results obtained from wind-tunnel tests of a low aspect ratio semispace wing model are presented. The tests were conducted to investigate potential transonic aeroelastic problems of vehicles having subsonic airfoil sections (e.g., the space shuttle). The model employed NACA 00XX-64 airfoil sections in the streamwise direction and had a 14° leading edge sweep angle. Aspect ratio, taper ratio, and average thickness were 4.0, 0.35, and 8 percent, respectively. The model was tested at Mach numbers from 0.6 to 0.95 at angles of attack from 0° to 15°.

Two zero lift flutter conditions were found that involved essentially single normal mode vibrations. With boundary layer trips on the model, flutter occurred in a narrow Mach number range centered at about Mach 0.90. The frequency and motion of this flutter were like that of the first normal mode vibration. With the trips removed flutter occurred at a slightly higher Mach number but in a mode strongly resembling that of the second normal mode.

Several instances of low torsional damping were observed at high angles of attack, but stall flutter was not encountered, except possibly at $M = 0.90, \alpha \approx 13°$. Maximum buffet loads occurred at angles of attack between 10° and 14°. Quantitative results for the maximum wing root bending moments due to buffet are presented in a form suitable for scaling.

INTRODUCTION

Wing and tail surfaces considered for the space shuttle orbiter have relatively thick airfoil sections that are generally associated with subsonic flight (ref. 1). Wings having such airfoil sections are not normally flown above M_{cr}; as a result little information is available concerning the transonic flutter behavior of thick wings. What information there is has been obtained from wind-tunnel tests of aeroelastic models since the unsteady viscous, mixed-flow problem associated with transonic flutter is not presently solvable by analytic means.

Flutter and buffet results from an aeroelastic model of one of the early Manned Spacecraft Center straight wing concepts are reported in reference 2. This wing had NACA 00XX-64 airfoil sections, an average spanwise thickness ratio of 12 percent, and an aspect ratio of 7. Wind-tunnel tests of the model revealed an unusual zero lift flutter behavior that occurred over a narrow transonic Mach number range, at quite low dynamic pressures, and at a frequency nearly identical to the first mode still-air vibration frequency. The present investigation was undertaken to determine if a thinner, lower aspect ratio wing model having the same airfoil shape would experience the

same type of dynamic instability. In addition, tests were conducted at sufficiently large angles of attack to determine the stall flutter and buffet characteristics of the model.

WIND TUNNEL

The tests were conducted in the Ames 11- by 11-Foot Transonic Wind Tunnel. This facility is a closed return slotted-throat, variable-pressure tunnel with an operating range of $51 \leqslant p_t \leqslant 220$ kN/m^2 ($15 \leqslant p_t \leqslant 65$ in.-Hg), where p_t is the total (stagnation) pressure. The variations in free-stream dynamic pressure and Reynolds number with tunnel total pressure are shown in figures 1 and 2, respectively.

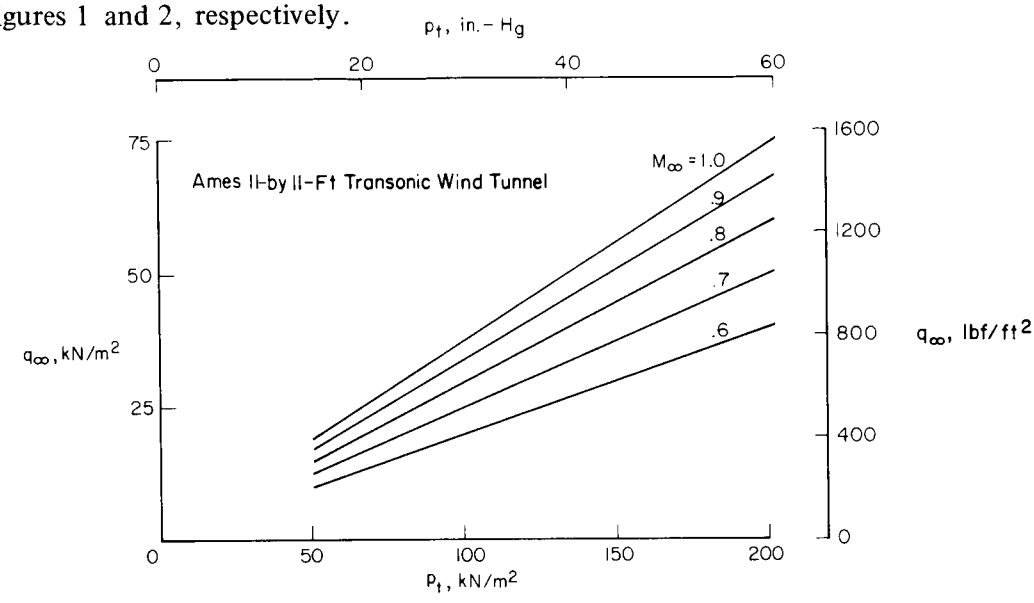

Figure 1.– Variation in free-stream dynamic pressure with total pressure.

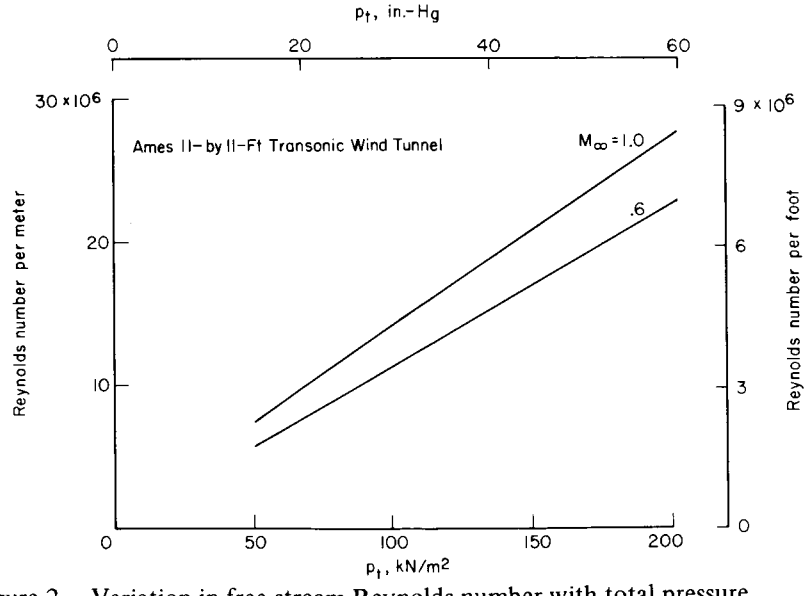

Figure 2.– Variation in free-stream Reynolds number with total pressure.

GEOMETRY AND CONSTRUCTION

Figure 3 shows the wing planform geometry. Wing construction details are illustrated in figure 4. The airfoil sections were NACA 00XX-64 profiles parallel to the flow with maximum thickness ratios varying from 9-1/3 percent at the root to 6-2/3 percent at the tip, giving an average thickness of 8 percent. The load-carrying structure consisted of a fiberglass-epoxy skin laid over a lightweight foam interior, and a birch spar at the 20 percent chord position. The spar and a skin thickness change at 30 percent chord were incorporated in the wing to adjust the chordwise positions of the section elastic axis and center of gravity. Spar dimensions and skin thicknesses varied linearly along the semispan between the values given at $y/L = 0$ and 1.

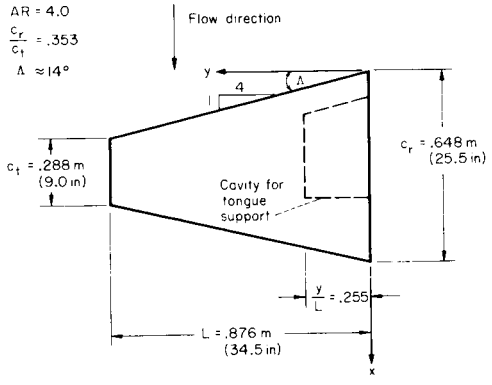

Figure 3.– Wing planform geometry.

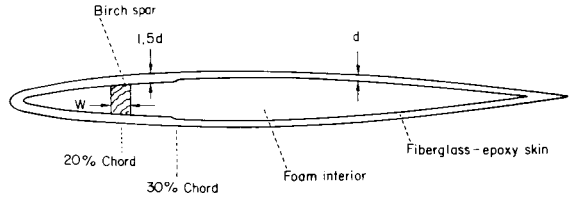

Spanwise position	Airfoil section (parallel to flow)	d	W
y/L = 0	NACA 009.3-64	.19 cm (.075 in.)	2.2 cm (.85 in.)
y/L = 1	NACA 006.7-64	.051 cm (.020 in.)	.45 cm (.18 in.)

Figure 4.– Airfoil section construction.

The model was mounted on a tapered steel tongue that matched a tapered cavity in the base of the model. A schematic of the wing support system is shown in figure 5. When the tongue was fully inserted into the cavity it fit snugly against the mating surfaces except at six slots, 2.54 cm (1 in.) wide. These slots provided clearance for wire-resistance strain-gage bridges that were bonded to the tongue at $\bar{y} = y/L = 0.18$. Separate bridges were aligned for both torsion and bending measurements. Figure 6 shows the model mounted in the wind tunnel. The large fiberglass fairings at the wing root covered clamping bolts used for tightly securing the wing to the tongue.

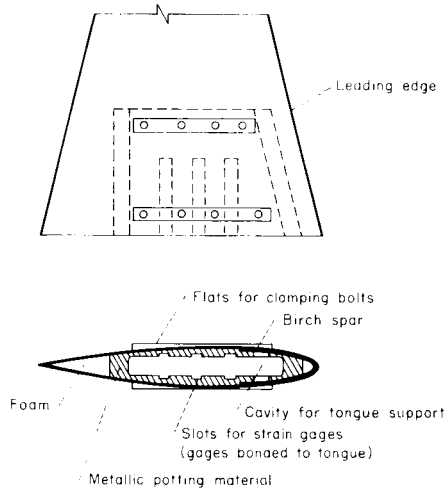

Figure 5.– Schematic of wing support system.

Except where noted, all testing was performed with boundary-layer trips located 5.7 cm (2-1/4 in.) from the model leading edge. The trips were 3.2 mm (1/8 in.) wide strips of 0.25 mm (0.010 in.) diameter glass spheres and there were approximately 40 spheres per cm (100/in.) of trip length. The model was covered with a white mixture of highly viscous oil and titanium dioxide to indicate flow patterns. Flow patterns observed at $\alpha = 0°, M = 0.6$, showed that the flow was nearly two-dimensional over the wing surface and was apparently little affected by the bolt cover fairings.

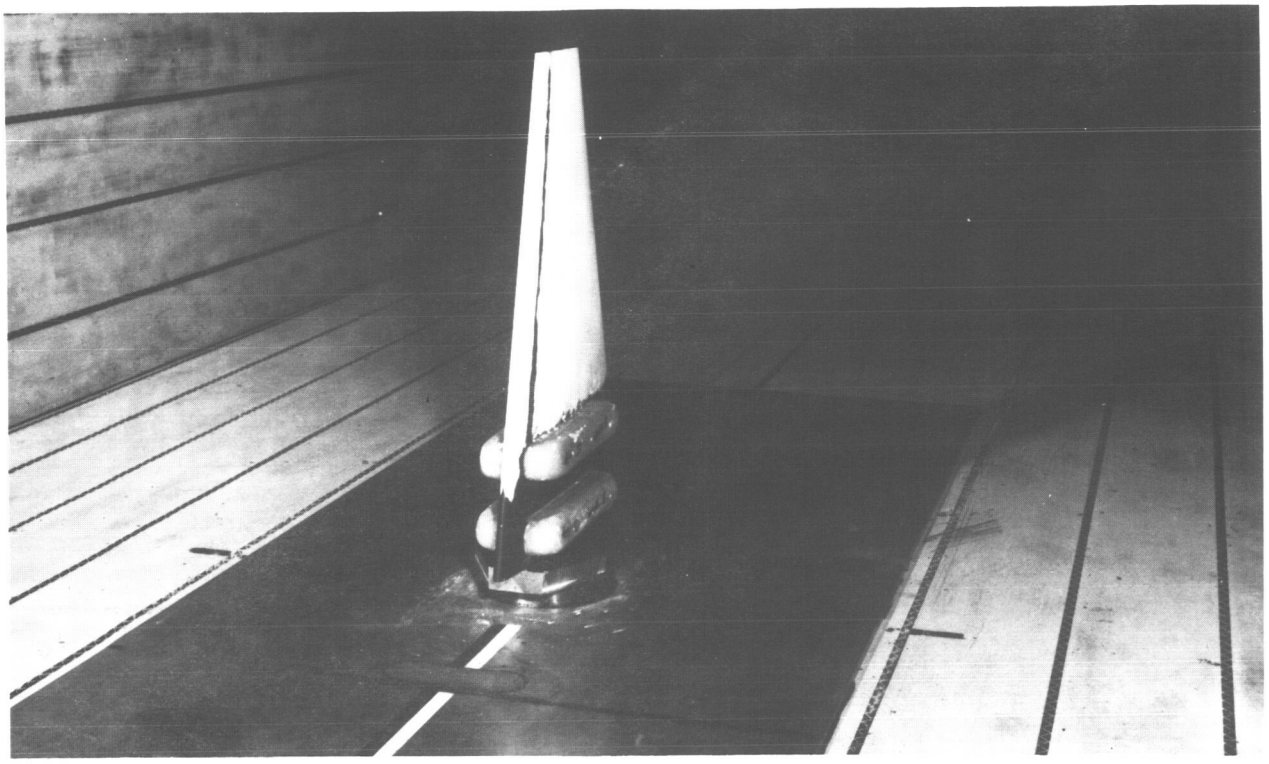

(a) 3/4 front view.

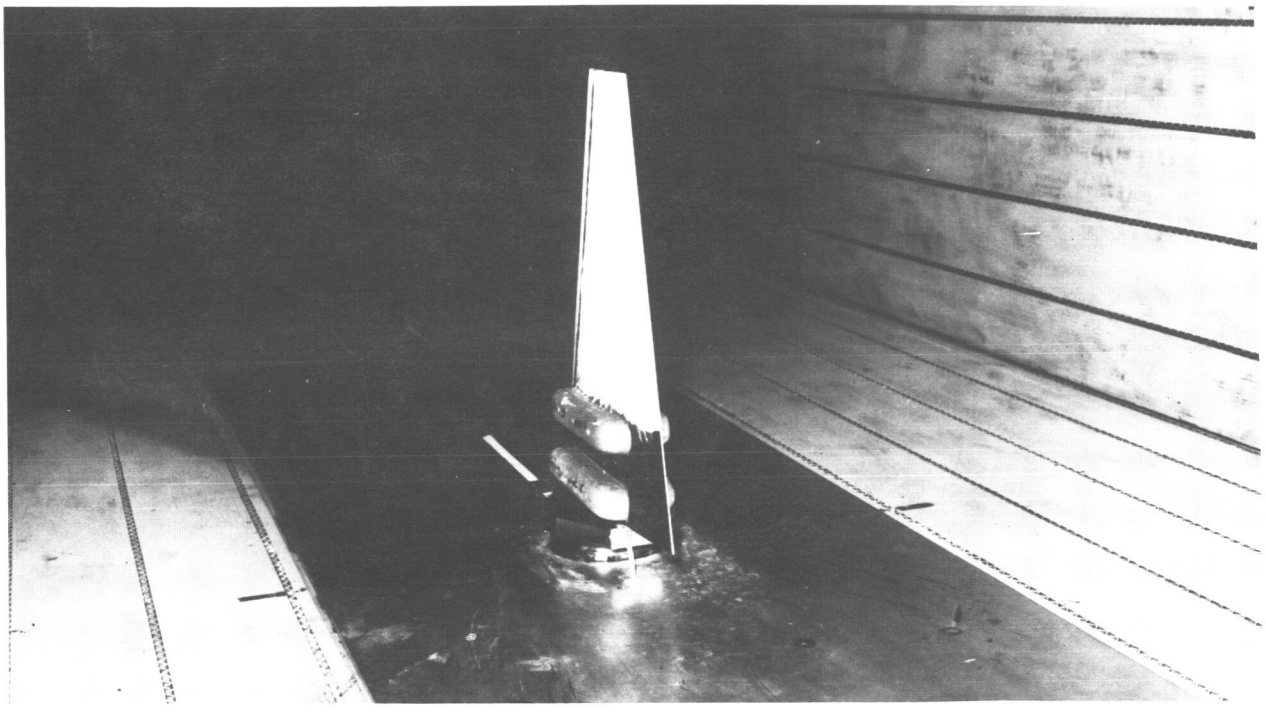

(b) 3/4 rear view.

Figure 6.– Model mounted in Ames 11- by 11-Foot Transonic Wind Tunnel.

Elastic and Mass Properties

The model was designed to have the same scaled strength as the $AR = 7$ model described in reference 2. The spanwise variation of the section bending stiffness (EI) and the bending-to-torsion stiffness ratio (EI/GK) for the model is shown in figure 7 for sections parallel to the flow. These values for EI and GK were computed from the wing cross section geometry and using $E = 14$ GN/m^2 (2.0×10^6 lbf/in.^{2}) for the fiberglass skin and birch spar and $G = 4.1$ GN/m^2 (0.60×10^6 lbf/in.^{2}) for the fiberglass. The rigidity of the foam and the torsional rigidity of the spar were neglected. Using these stiffnesses, spanwise deflections due to a tip load, and spanwise angles of twist due to a tip-torque were computed from engineering beam theory.[1] These bending and twisting displacements are shown in figure 8(a) and (b), respectively. Measured deflections obtained from static bending and torque tests are also shown. Angles of twist were measured in planes perpendicular to the 40 percent chord line. The bending deflections were measured at 40 percent chord positions with the tip load at 40 percent chord. The fairly good agreement between the measured and computed deflections indicate that the model stiffness properties given in figure 8 are reasonably accurate.

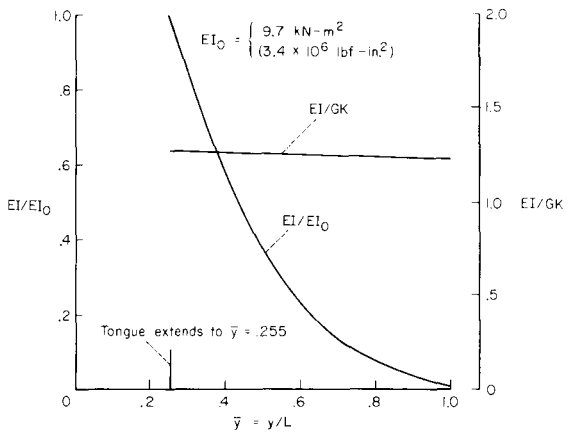

Figure 7.– Spanwise variation of elastic stiffnesses.

Additional model section properties, computed from the chordwise distribution of mass and bending stiffness, are given in table 1 (c is the local chord length). The mass ratio μ of the portion of the model outboard of the tongue is

$$\mu = \frac{16}{\rho_\infty}\left(\frac{310 \times 10^{-4}}{\rho_\infty}\right)$$

where ρ_∞ is the free-stream air density in kg/m^3 (slugs/ft^3). The mass ratio is plotted versus Mach number in figure 9 for $p_t = 51$ kN/m^2 (15 in.-Hg). Also shown is the variation in first mode reduced frequency, $k_1 = b\omega_1/V_\infty$. (Model values of μ and k are required to predict full-scale aerodynamic damping as explained in the section on buffeting.)

TABLE 1.– MODEL SECTION PROPERTIES

	$\bar{y} = 0.255$	$\bar{y} = 1.0$
Distance from leading edge		
to elastic axis	0.375c	0.383c
to center of gravity	0.422c	0.433c
Radius of gyration		
about elastic axis	0.290c	0.292c

[1] Due to the low aspect ratio and plate like geometry of the model, the bending deflections were computed by replacing EI with $EI/(1-\nu^2)$, $\nu = 0.3$. Also, equation (g) of reference 3 (p. 65) was used to correct approximately the twisting deflections for wing root warping restraint. (This correction gave a 15 percent decrease in angle of twist at the wing tip.)

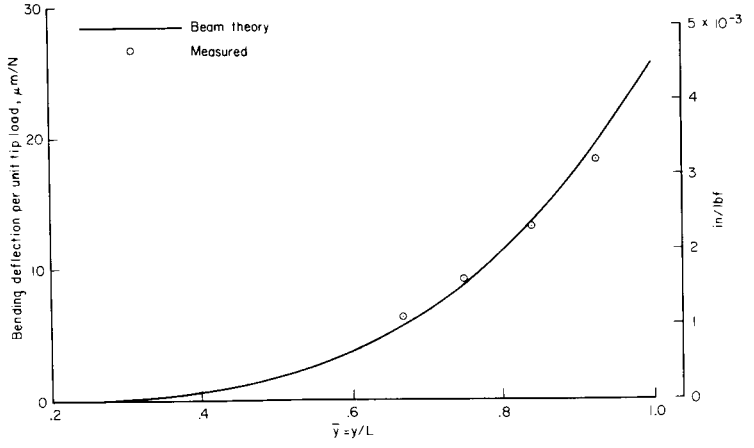

(a) Bending deflection due to concentrated force at wing tip.

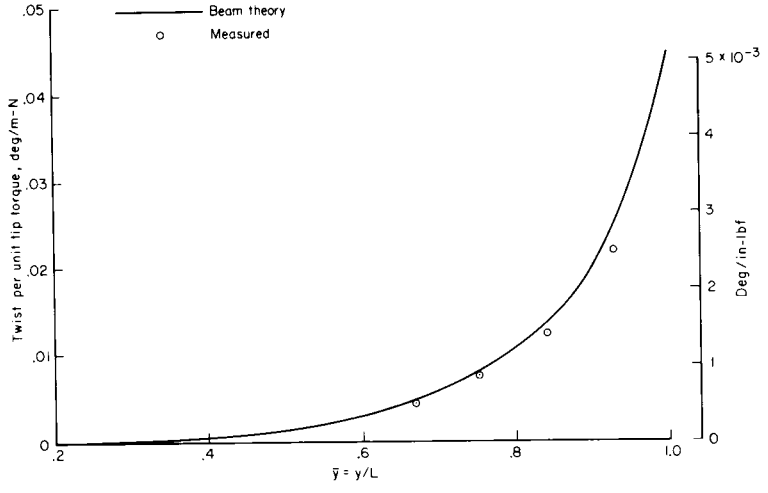

(b) Angle of twist due to a concentrated torque at wing tip.

Figure 8.– Static deformation behavior.

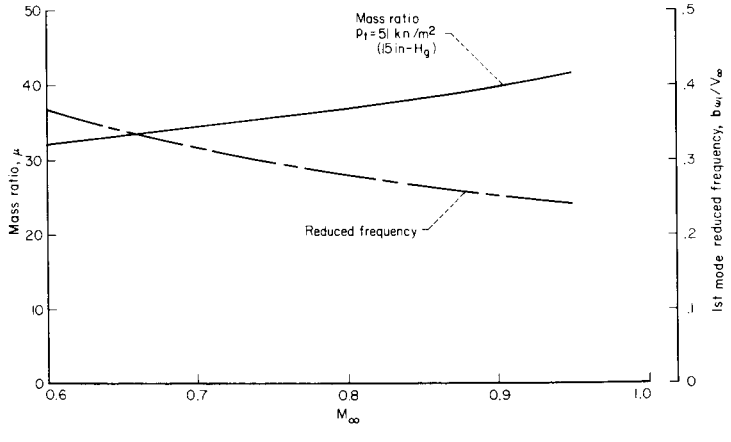

Figure 9.– Variation in mass ratio and reduced frequency with Mach number.

Still-Air Vibration Characteristics

Values of still-air frequencies and damping ratios are given in table 2 for the first three normal vibration modes of the model. Mode 1, a beam-like fundamental bending mode, is shown in figure 10(a) being driven at reasonance by an air-jet exciter. Modes 2 and 3 are plate-like modes as shown by the node line patterns in figures 10(b) and 10(c), respectively.

TABLE 2.– FREQUENCY AND DAMPING RATIO

	Strongback installation		Wind tunnel installation	
Mode number	Frequency, Hz	Damping ratio, percent	Frequency, Hz	Damping ratio, percent
1	72.5	0.5	70.2	0.75
2	160	0.95	- - -	- - -
3	205	0.88	- - -	- - -

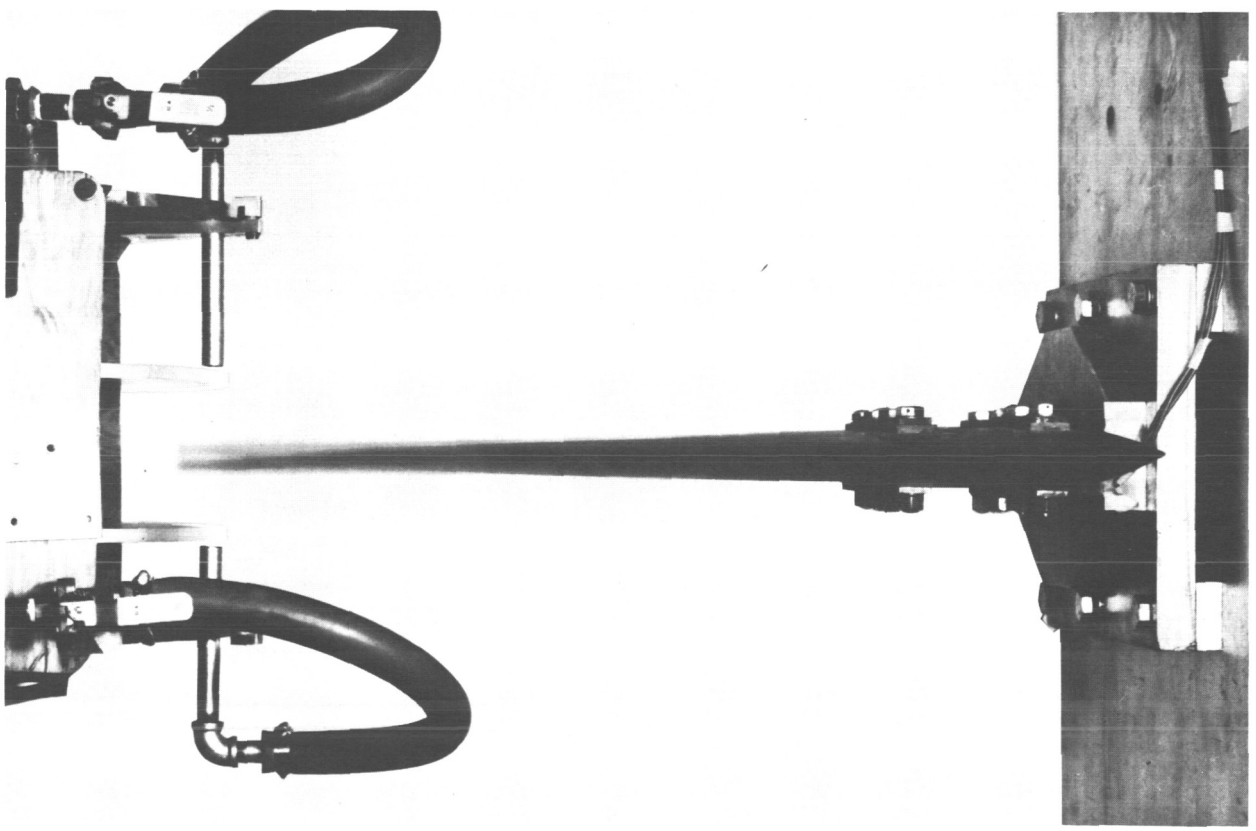

(a) First mode; $f = 72.5$ Hz.

Figure 10.– Normal mode vibration shapes.

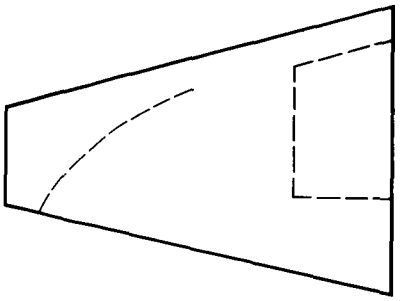

(b) Second mode; $f = 160$ Hz.

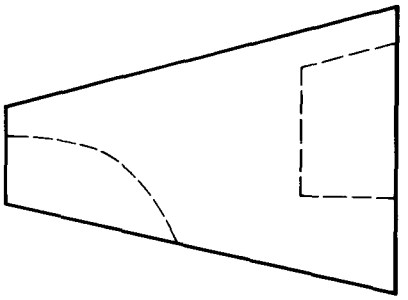

(c) Third mode; $f = 205$ Hz.

Figure 10.– Concluded.

TEST PROCEDURE AND DATA REDUCTION

Previous tests (ref. 2) of the $AR = 7$, $t/c = 12$ percent flutter model having the same airfoil profile as the present one revealed a very unusual type of transonic flutter, which occurred only over a narrow Mach number range. Because of this flutter sensitivity to Mach number, the present test was conducted in the following manner:

1. Zero-lift flutter search.– With $\alpha = 0°$, and the tunnel at the lowest operating pressure, Mach number was varied between 0.6 and 0.95. (Limit amplitude flutter was encountered in the vicinity of $M = 0.90$, but the model had sufficient strength to allow the flutter region to be traversed without damage.) Total pressure was then increased and the Mach number survey repeated.

2. Stall flutter and buffet test ($\alpha > 0°$).– For $\alpha > 0°$, all tests were conducted at the lowest tunnel operating pressure so as to keep static airloads to a minimum. At fixed Mach numbers, the angle of attack was varied from 0° to 15°.

The above procedure was followed with boundary-layer trips in place. After completion of the stall flutter and buffet tests these trips were removed and the zero lift flutter search was repeated at a low tunnel pressure. With the trips removed, no evidence of flutter was found near $M = 0.90$ so pressure was then increased while Mach number was held between 0.90 and 0.93. Eventually, a pressure was reached at which flutter was again encountered. As discussed later, this flutter was of a different nature than that found with the trips in place and the model was destroyed.

The wing motion was continuously monitored by oscilloscope displays of the strain-gage signals and by a television display from a camera mounted above the wing tip. High-speed motion pictures of the wing motion were taken at several test conditions.

Throughout the test, the strain-gage signals were continuously recorded on magnetic tape. During fixed test conditions, the time histories of the model response were recorded over a 135-sec period. The dc components from the torsion and forward bending gage were filtered electronically before being recorded; this made the entire range of the recording system usable for the model dynamic response. The complete signal (ac + dc) from the rear bending gage was recorded so that comparisons could be made of the dynamic and static bending loads on the model.

The recorded data were analyzed from measurements of the overall rms, frequency spectra, autocorrelations, and oscillograph records of the time histories.

The still-air frequency and damping ratio of the first bending mode were measured several times during the test and were unchanged. Wind-on damping ratios were obtained from envelopes of the autocorrelation functions (ref. 4).

RESULTS AND DISCUSSION

Zero-Lift Flutter

At $\alpha = 0°$ the model was tested at total pressures ranging from 51 kN/m^2 to 186 kN/m^2 (15 in.-Hg to 55 in.-Hg) at Mach numbers from 0.6 to 0.95. Over this pressure range, the model was flutter free except in a narrow Mach number range in the vicinity of $M = 0.90$. The characteristics of this flutter are described below. Except where noted, all results are for the model with boundary-layer trips attached.

Response levels.– Figure 11 shows the effect of Mach number on the rms signal level σ_B of the bending gage at the lowest tunnel operating pressure. Evidence of flutter at $\alpha = 0°$ is indicated by the large rise in response near $M = 0.90$. Note that this response is completely eliminated with the model at $\alpha = 2°$.[2] At higher pressures, the general character of the response was the same as shown in figure 12, but the magnitude of σ_B at $M = 0.90$ decreased as p_t increased. The same behavior was observed on the thicker, higher aspect ratio model of reference 2.

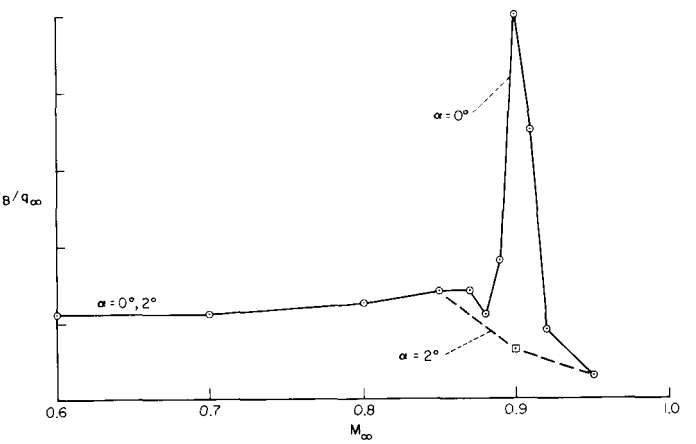

Figure 11.– Effect of Mach number on dynamic response; $p_t = 51$ kN/m^2 (15 in.-Hg).

Frequency spectrums.– Frequency spectrums of the bending and torsion gage signals are shown in figure 12 for $\alpha = 0°$ and 2° at $M = 0.90$. At $\alpha = 0°$, both the bending and torsion gages show a predominant frequency component at about 72 Hz, a value nearly identical to the still-air first mode vibration frequency of the model. At $\alpha = 2°$, the 72 Hz component still predominates in the bending-gage spectrum (but at a much lower level), and it is barely noticeable in the torsion-gage spectrum.

Damping.– Net damping levels (aerodynamic plus structural) associated with the bending motion of the first mode frequency are shown in figure 13 where ζ_{1B}, the ratio of damping to critical damping, is plotted against Mach number ($p_t = 51$ kN/m^2 (15 in.-Hg)). These damping ratios were obtained by passing the bending gage signals through a 65- to 85-Hz bandpass filter and computing the autocorrelation of the resulting signal. For $\alpha = 0°$, the net damping is seen to be less

[2] A careful Mach number survey at $\alpha = 2°$ ($0.85 \leqslant M \leqslant 0.95$) showed no indication of flutter.

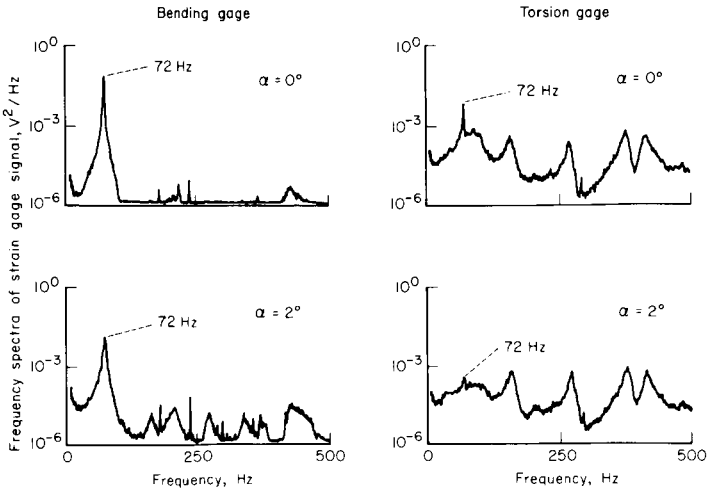

Figure 12.– Frequency content of strain gage signals; p_t = 51 kN/m² (15 in.-Hg); M_∞ = 0.90.

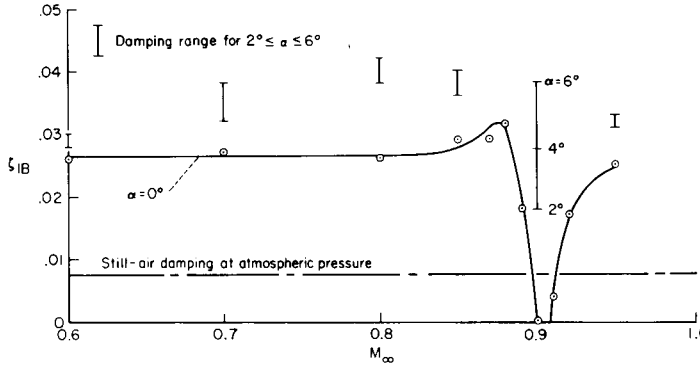

Figure 13.– Effect of Mach number and angle of attack on damping; p_t = 51 kN/m² (15 in.-Hg).

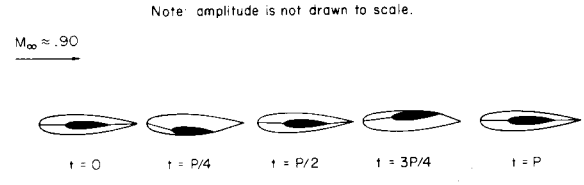

Figure 14.– Flutter motion with boundary-layer trips attached.

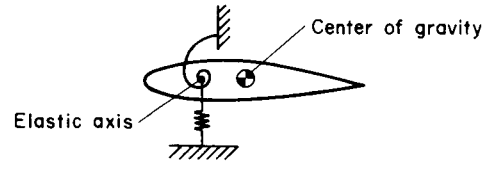

Sketch (a)

than the still-air value in the narrow Mach number range centered at about M = 0.90. Thus, the large response level of figure 11 is due to negative aerodynamic damping (i.e., flutter) rather than to a severe buffet type input. Ranges in damping for $2° \leqslant \alpha \leqslant 6°$ are also shown in figure 13. For α = 2° the aerodynamic damping decreases in the vicinity of M = 0.90 but flutter does not occur.

Wing motion.– The limit amplitude flutter motion was established with the aid of high-speed motion pictures. One cycle of this motion at quarter-cycle intervals is illustrated in figure 14. The wing bends and twists in phase, the nose-up attitude occurring when the wing is bent down. (The same flutter motion was observed on the thicker, higher aspect ratio wing of ref. 2.) Measurements from high-speed motion pictures of the motion indicate the maximum double amplitude wing tip displacement (measured at 0.4 c_t) and rotation were approximately 2.54 cm (1 in.) and 2°, respectively.

It is of interest to compare the flutter motion with the free-vibration motion of the two-degree-of-freedom system sketched below. If the center of gravity and the elastic axis coincide, one of the two normal modes of this system vibrates in pure translation at a frequency ω_h while the other vibrates in pure rotation at a frequency ω_θ. However, if the center of gravity is aft of the elastic axis (as in the case of the wind tunnel model, and as shown in sketch (a)) the normal modes contain contributions from both degrees of freedom. In this case, and for $\omega_h < \omega_\theta$, the fundamental (lowest frequency) normal mode has the same phasing (between the translational and rotational degrees of freedom) as the flutter motion shown in figure 14 (ref. 5). This similarity in phase, together with the nearly identical values of the flutter and fundamental normal mode frequencies of the

model, strongly suggests that the motion-induced aerodynamic forces are able to feed energy into a *single* normal mode. (This is in contrast to "classical" flutter, which usually involves the participation of two or more normal modes.)

Speculation concerning the flutter mechanism.– Several types of single degree of freedom flutter have been predicted on the basis of unsteady potential flow theory (ref. 6). Other types, however (e.g., control surface buzz (ref. 7), stall flutter (ref. 8), and hammerhead configuration instabilities (ref. 9)), are generally attributed to nonpotential flow characteristics such as oscillating shock-wave boundary layer interaction and unsteady separated flow.

The single mode-like flutter behavior in the present investigation is completely analogous to that of the 12 percent thick, aspect ratio = 7 model described in reference 2. The instability of the 12 percent thick model, which occurred at $0.84 < M < 0.86$, appeared to be associated with the onset of shock stall. (Oil flow photos indicated a large region of shock-induced separated flow at $M \approx 0.85$, the extent of which was extremely sensitive to small (0.01) changes in Mach number.) This possibility is consistent with the present results since the 8 percent thick model would be expected to encounter shock stall at a higher Mach number.

The restriction of the instabilities to narrow Mach number ranges is also an indication of shock stall onset. At Mach numbers greater than critical, static lift and pitching moment coefficients of airfoils similar to those used on the present model (and on the 12 percent thick model of ref. 2) can display large variations in magnitude over narrow Mach number ranges (refs. 10 and 11). The chordwise static pressure data of reference 11 indicate these variations are most extreme at the Mach number corresponding to the onset of shock-induced trailing edge separation (M_{sep}). At this condition (i.e., where the flow is transitional between attached and separated) there is likely to be a strong interdependence between wing motion, shock position and strength, and boundary layer separation. For example, the upper and lower surface shocks, in conjunction with the rotational motion[3] of the wing (due to a normal mode vibration), might cause the boundary layers on opposite sides of the wing to alternate between attached and separated flow. Thus, self-induced oscillating forces would be produced in synchronism with the wing motion. With the proper magnitude and phase, these oscillating forces could do enough positive work per cycle to balance the energy loss due to structural damping. An instability produced by such a mechanism would be expected to occur only in a narrow Mach number range centered about M_{sep} since at slightly lower Mach numbers the flow would be predominately attached, whereas at slightly higher Mach numbers the flow would be fully separated between the trailing edge and the upstream shock-induced separation point.

In the flutter mechanism postulated above, the fluctuating forces are considered to act in synchronism with the motion of a normal mode vibration. This would explain the flutter frequency being nearly identical to a normal mode frequency. (Some difference in frequency would be expected due to aerodynamic mass and stiffness effects.) However, the ability of a particular mode to become unstable probably requires a reasonable fit between the spatial pattern of the normal mode motion and the spatial pattern of the fluctuating surface pressures. This implies that normal

[3]Unpublished test results for an aluminum skin, honeycomb core version of the $AR = 7$ fiberglass model of ref. 2 indicate the rotational degree of freedom is very important. The aluminum model was approximately three times stiffer in torsion than the fiberglass model but had approximately the same bending stiffness and first mode frequency. This torsionally stiffer model was flutter free at all test conditions where the fiberglass model experienced flutter.

modes other than the fundamental could also become unstable by altering the spatial distribution of the separated flow. Evidence that such behavior is possible is given in the following section.

Natural transition.– At a given tunnel condition (fixed Reynolds number per unit length), removal of the boundary-layer trip should change the location of boundary layer transition and the boundary layer thickness from that of the tripped model. Changes in tunnel Reynolds number would produce additional changes in these properties. The attendant effect on the occurrence of, and the spatial distribution of, shock-induced flow separation (refs. 12, 13, 14) and the resulting forces, might then alter the wing flutter characteristics. Reynolds number variations, for example, are known to affect static pitching moments at supercritical Mach numbers (see ref. 15, figs. 4 and 6).

With the boundary-layer trips removed, a Mach number sweep at $\alpha = 0°$ from $M = 0.6$ to 0.95 at $p_t = 84$ kN/m^2 (25 in.-Hg) showed no evidence of flutter. The change in wing damping due to removal of the boundary-layer trips is shown in figure 15. Damping ratios associated with the fundamental mode frequency are given at two total pressures for the wing with trips (open symbols), and at the higher of the two pressures for the wing without trips (dark symbols). With the trips in place the aerodynamic damping becomes negative at both pressures, although confined to a narrower Mach number range at the higher pressure. At this higher pressure, but with the trips removed, there is a small decrease in damping near $M = 0.9$, but flutter does not occur. Thus, Reynolds number effects apparently play a crucial role in the flutter mechanism.

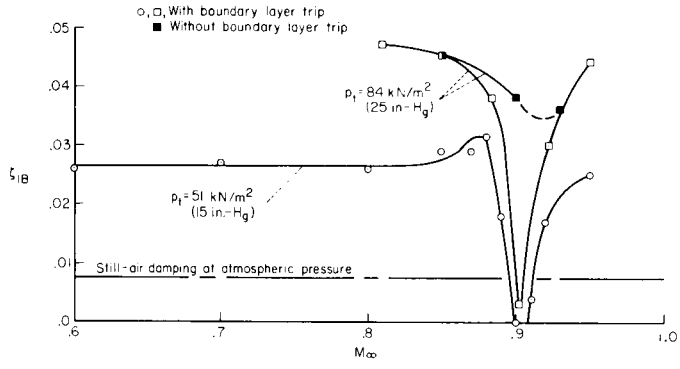

Figure 15.– Effect of total pressure and boundary-layer trip on damping; $\alpha = 0°$.

Since the model without trips was flutter free at $p_t = 84$ kN/m^2 (25 in.-Hg), Reynolds number (as well as dynamic pressure) was increased by increasing p_t, the Mach number being held between 0.90 and 0.93. Flutter was encountered at $p_t = 154$ kN/m^2 (45.7 in.-Hg), $M = 0.92$. No flutter occurred at this test condition when the boundary-layer trips were in place; thus, the flutter encountered without trips is evidently due to a Reynolds number effect rather than to the increasing dynamic pressure. The model was destroyed at this condition just after several seconds of high-speed motion pictures were taken of the flutter motion.

Two frames from the motion picture film are reproduced in figure 16(a). These frames show the model near its extreme flutter amplitudes. At the wing tip, the amplitude of the leading edge motion is greater than that of the trailing edge. Also, the trailing edge has a nodal point a short distance inboard of the tip section. Figure 16(b) is a sketch of this flutter motion; note that it is very similar to the second still-air normal vibration mode of the model shown in figure 10(b).

The flutter frequency in this case was 145 Hz, a value about 10 percent less than the second mode still-air frequency of 160 Hz. The 160 Hz still-air value is evidently decreased by aerodynamic mass and stiffness effects, as evidenced by the data in table 3, which gives frequencies corresponding

to the predominant peaks in the strain-gage signal spectrums for various flow conditions. For $M \leqslant 0.91$, only the first mode frequency (72 Hz) is predominant. For $M \geqslant 0.92$, the second mode frequency is also apparent; at the low total pressure it has a value of 160 Hz (same as the still-air value) for the model with trips, and a value of 155 Hz for the model without trips. At the higher total pressure these values have been reduced by 10 Hz. Thus, the 145 Hz flutter frequency for the model without trips can be traced to the model's second still-air normal mode frequency. This finding, together with the similarity between the second normal mode motion and the flutter motion, is again indicative of a *single mode* type of instability.

The above experimental results indicate that different normal modes can become unstable due to the presence or absence of a boundary-layer trip. This supports the contention that the ability of a particular mode to become unstable is influenced by the spatial distribution of the boundary layer characteristics and the attendant effects on the onset of shock stall.

Implication of results.– The results of the present investigation and of reference 2 demonstrate that either high or low aspect ratio straight wings with subsonic airfoils are susceptible to flutter over narrow transonic Mach number ranges. The results obtained apply only to the configurations tested, but they raise concern for other wing and tail geometries since the flutter is associated with single mode type instabilities rather than with coupled mode interactions. For example, the node line pattern of the unstable second mode for the $AR = 4$ model (fig. 10(b)) resembles that expected for delta wing configurations.

Several aspects of these instabilities are of secondary importance to more usual flutter behavior. For one thing, the instabilities can apparently be prevented by flying at moderately small angles of attack. Thus, the problem could be avoided for a wing (but not for nonlifting tail surfaces). Second, the occurrence of flutter in very narrow Mach number ranges and the limit amplitude behavior may make it possible (but not necessarily acceptable) to fly through such flutter regions with no structural damage. Accummulated fatigue damage could be a major consideration, however.

These Mach number sensitive results indicate that very close attention should be paid to small Mach number

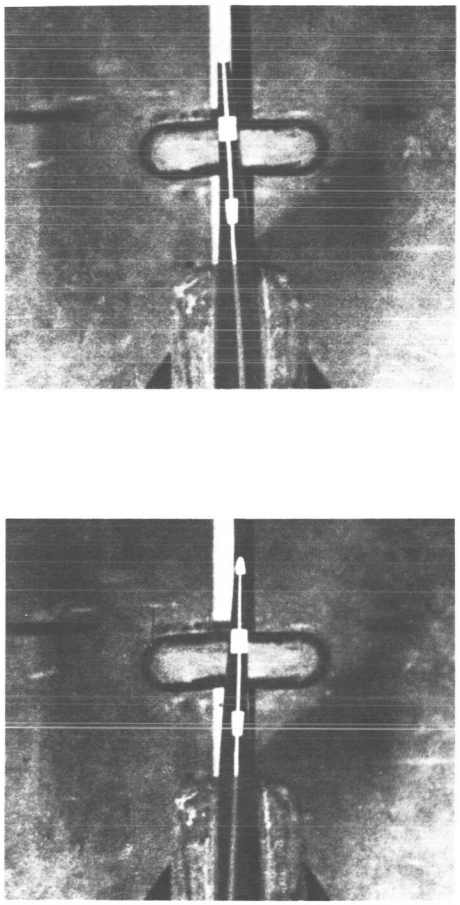

(a) Frames from high speed motion pictures; flow is from top to bottom of picture.

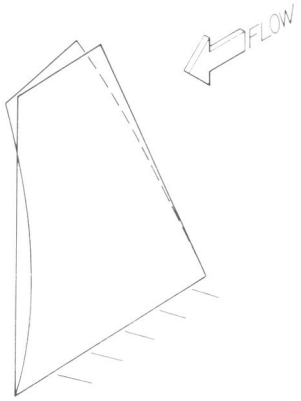

(b) Sketch of flutter mode shape.

Figure 16.– Flutter motion with natural transition; $M_\infty = 0.92$, $p_t = 154\ \text{kN/m}^2$ (45.7 in.-Hg).

TABLE 3.– PREDOMINANT FREQUENCIES IN STRAIN-GAGE SIGNAL SPECTRUMS, Hz; $\alpha = 0°$

	With boundary-layer trips				Without boundary-layer trips			
	$p_t = 84$ kN/m^2 (25 in.-Hg)		$p_t = 152$ kN/m^2 (45 in.-Hg)		$p_t = 84$ kN/m^2 (25 in.-Hg)		$p_t = 154$ kN/m^2 (45.7 in.-Hg)	
	Bending gage	Torsion gage	Bending gage	Torsion gage	Bending gage	Torsion gage	Bending gage	Torsion gage
$M = 0.85$	72	None	72	None	---	---	---	---
$0.89 \leqslant M \leqslant 0.91$	72	72	72	72	72	None	---	---
$M = 0.92$	72;160	160	72[a]	150[a]	72;155	155	145	145
$M = 0.95$	72;160	160	72;150	150	---	---	---	---

[a]Value interpolated from frequencies at lower and higher total pressures.

variations in transonic flutter tests. Because of the demonstrated Reynolds number effects, consideration also should be given to simulating full scale boundary layer characteristics as closely as possible.

Buffet and Stall Flutter

The following results describe the dynamic response of the wing for angles of attack from 0° to 15° at Mach numbers from 0.6 to 0.95. All results were obtained at a total pressure of 51 kN/m^2 (15 in.-Hg) and with boundary-layer trips attached to the model.

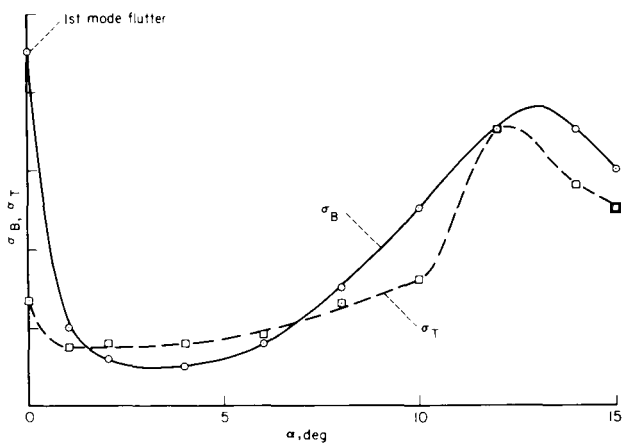

Figure 17.– Relative variation in rms bending and torsion gage signals with angle of attack; $M_\infty = 0.90$, $p_t = 51$ kN/m^2 (15 in.-Hg).

A measure of the dynamic response of the wing is given by the standard deviations of the bending and torsion gage signals σ_B and σ_T, respectively. An example of the relative variation in σ_B and σ_T with angle of attack is shown in figure 17, which is for $M = 0.90$. The large response at $\alpha = 0°$ is due to the first mode flutter condition discussed earlier and does not occur at Mach numbers slightly less than or greater than 0.90. Except for this $M \approx 0.90$ case, σ_B and σ_T remain relatively constant until some angle is reached at which a fairly rapid increase in response occurs as α increases. As shown in figure 17, σ_B and σ_T peak at relatively large angles of attack and then diminish as α increases further.

For each test Mach number, examination of the strain-gage frequency spectra at the angles of maximum response ($\alpha > 0°$) shows that σ_B (bending response) is almost entirely due to vibration at the first normal mode frequency, whereas σ_T (torsion response) is primarily due to the second

mode vibration. (The spectrum peaks at these vibration frequencies were one to two orders of magnitude larger than those at any other frequency.)

Net damping ratios for the first (predominantly bending) and second (predominantly torsion) modes are denoted as ζ_{1B} and ζ_{2T}, respectively,[4] and are shown in figure 18 for $M = 0.90$. For $10° \leqslant \alpha \leqslant 15°$ ζ_{1B} has a constant value several times larger than the first mode still-air damping value. This implies that the $\alpha \approx 13°$ peak in σ_B (fig. 17) is due to an increase in dynamic load input and can be categorized as wing buffeting. The peak in σ_T, however, occurs where aerodynamic damping ζ_{2T} is near zero. Hence, the peak in σ_T is more closely associated with the wing being at, or near, a condition of stall flutter (ref. 16).

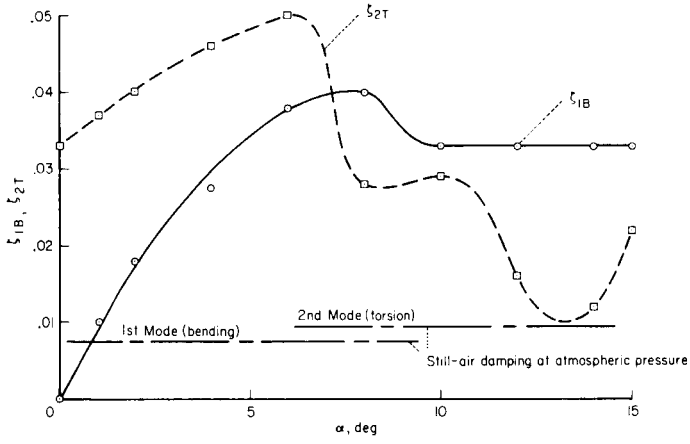

Figure 18.– Variation in damping ratio with angle of attack; $M_\infty = 0.90$, $p_t = 51$ kN/m² (15 in.-Hg).

The total wing response at large angles of attack can thus be regarded as a combination of buffeting and near stall flutter. However, in this case the buffet (relatively large damping) and stall flutter (low damping) phenomena can be fairly well distinguished since they affect different modes, which are well separated in frequency (i.e., response due to modal frequency overlap (ref. 17) is probably not significant). For convenience, then, the peaks in bending response (σ_B) will be referred to simply as buffeting.

A buffet region can be estimated from figure 17 and similar figures for other Mach numbers. For a given Mach number, the angle of buffet onset was determined as shown in figure 19. Figure 20 shows the approximate Mach number and angle of attack combinations at which the buffet boundary and maximum buffet intensity occur. At $M = 0.90$ the buffet onset angle is

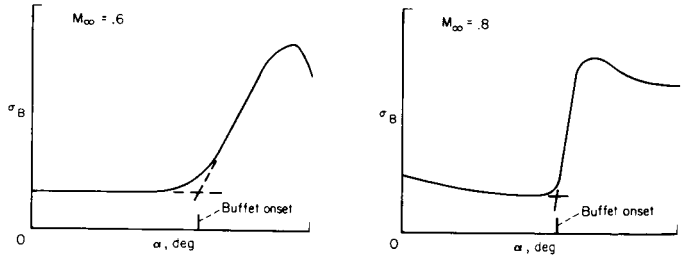

Figure 19.– Definition of buffet onset angle.

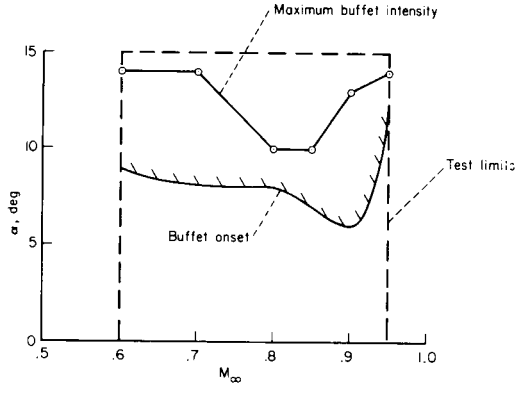

Figure 20.– Buffet onset boundary and angles of maximum buffet intensity; $p_t = 51$ kN/m² (15 in.-Hg).

[4] The damping ratios, ζ_{1B}, ζ_{2T} for modes 1 and 2 were obtained by bandpassing the strain-gage signals about the first and second mode frequencies, respectively, and computing the autocorrelations of the resulting signal.

approximately 6°, a value near that at which $(\zeta_{1B})_{max}$ occurs, (see fig. 18).[5] This behavior has been previously noted in reference 18 where ζ_{1B} was measured from flight data. Quantitative information concerning the points of maximum buffet intensity is given below in a form useful for predicting full-scale buffet loads.

The total wing root bending stress (static plus dynamic) is equal to the static stress times the factor $[1 + (\bar{M}_{dyn}/\bar{M}_{static})]$ where $\bar{M}_{static}$ and $\bar{M}_{dyn}$ are the static and dynamic wing root bending moments, respectively. As mentioned earlier, the dynamic bending gage signal $\sigma_B \propto \bar{M}_{dyn}$ is due almost entirely to the first mode vibration. Consequently, full scale values of $\bar{M}_{dyn}/\bar{M}_{static}$ can be predicted from model values by the following buffet scaling relation (ref. 19):

$$\frac{(\bar{M}_{dyn}/\bar{M}_{static})^2 \text{ full scale}}{(\bar{M}_{dyn}/\bar{M}_{static})^2 \text{ model}} = \frac{[k_1/(\zeta_a + \zeta_s)] \text{ full scale}}{[k_1/(\zeta_a + \zeta_s)] \text{ model}} \tag{1}$$

where $k_1 = b\omega_1/V_\infty$ (first mode reduced frequency) and ζ_a and ζ_s are the aerodynamic and structural damping ratios (fraction of critical) associated with the first mode vibration frequency.[6] Use of the scaling relation for aerodynamic damping due to bending (ref. 20)

$$(\zeta_a \mu k_1)_{\text{full scale}} = (\zeta_a \mu k_1)_{\text{model}} \tag{2}$$

and the fact that $\omega^2 \propto (1/\ell^4)\,(EI/m_w)_o$, allows equation (1) to be written as

$$R = \left[\frac{\bar{M}_{dyn}}{\bar{M}_{static}} \sqrt{\frac{(1 + \zeta_s/\zeta_a)}{(EI_o/\ell^4 q)}}\right]_{\text{model}} = \left[\frac{\bar{M}_{dyn}}{\bar{M}_{static}} \sqrt{\frac{(1 + \zeta_s/\zeta_a)}{(EI_o/\ell^4 q)}}\right]_{\text{full scale}} \tag{3}$$

This form may at times be more useful than equation (1) since ζ_s/ζ_a is often small compared to unity. The moment ratio then scales (approximately) by the ratio of $\sqrt{EI_o/\ell^4 q}$, a term that is more readily estimated than k_1 and $\zeta_a + \zeta_s$ for the full-scale wing since it depends on static rather than dynamic structural properties.

Because buffeting is a random type process, $\bar{M}_{dyn}$ can fluctuate considerably from its root-mean-square value. In the present investigation, the peak values of the dynamic bending moment ($\bar{M}_{peak\text{-}dyn}$, fig. 21) experienced by the model were determined from bending gage oscillograph records representing 120 sec of the time history ($\approx$ 8500 cycles[7] at the first mode frequency of the wing). Model values of R (eq. (3)) corresponding to $\bar{M}_{peak\text{-}dyn}$ are given in figure 21 for the Mach

[5] The peak in ζ_{2T} at $\alpha = 6°$ for $M = 0.90$ is considered to be coincidental. Comparison of buffet onset angles with angles of $(\zeta_{2T})_{max}$ at other Mach number shows no apparent correlation except that $(\zeta_{2T})_{max}$ always occurred at angles less than or equal to the buffet onset angles (e.g., 50 percent less at $M = 0.60$).

[6] The scale relation given by equation (1) requires the model and full scale wings to have similar geometry, and similar generalized modal characteristics and reduced frequencies pertinent to the first vibration mode.

[7] For a stationary narrow-band Gaussian process with zero mean, the expectancy of exceeding a $|3\sigma|$ value would be once every 45 cycles (ref. 21).

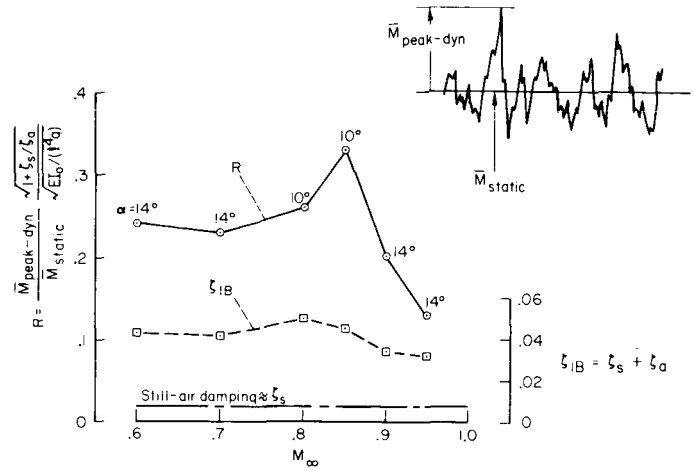

Figure 21.– Peak wing-root bending moment and first mode damping at angles of maximum buffet intensity.

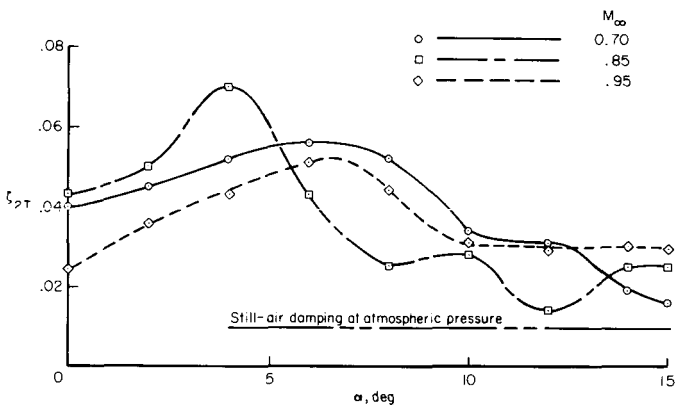

Figure 22.– Variation in second mode torsional damping ratio with angle of attack; p_t = 51 kN/m² (15 in.-Hg).

number angle of attack combinations of maximum buffet intensity. The first mode damping ratios used to compute R are also given in this figure (ζ_s was taken as the still-air damping value). The model values for ζ_a can be scaled to full scale values by use of equation (2) and the value for μ and k_1 given in figure 9.

As mentioned earlier, tendencies toward stall flutter instabilities can be distinguished from the forced buffet response by examining the variation in ζ_{2T} with angle of attack. This variation was shown in figure 18 for $M = 0.9$ and is shown in figure 22 for three additional Mach numbers. In each case values of ζ_{2T} less than the still-air damping value would correspond to negative aerodynamic damping and a condition of stall flutter (or near stall flutter). For the angle of attack and Mach number range considered ($0 \leqslant \alpha \leqslant 15°$. $0.6 \leqslant M \leqslant 0.95$), the aerodynamic damping, although low at some test conditions remains positive (stabilizing) with the possible exception of $M = 0.90$, $\alpha \approx 13°$. Thus, stall flutter is not indicated except possibly in the vicinity of $M = 0.9$, $\alpha = 13°$.

It is noted that the parameter $b\omega_2/a$ (a = speed of sound) had a value varying from 0.50 to 0.52 for $0.6 \leqslant M_\infty \leqslant 0.95$. (A *rough* rule of thumb is that a value greater than about 0.5 for this parameter is sometimes indicative of a stall-flutter free wing (ref. 8).)

CONCLUDING REMARKS

Experimental results have been presented for the transonic flutter and buffet behavior for a low-aspect-ratio wing having an NACA 00XX-64 airfoil shape with a 9.3 percent thickness at the root and a 6.7 percent thickness at the tip. The model was tested at Mach numbers from 0.6 to 0.95, at angles of attack from zero to 15°, and at various dynamic pressures. The following results are noted:

1. Single-mode type flutter instabilities occurred at near zero angle of attack. These instabilities were extremely sensitive to both Mach number and Reynolds number and appear to be associated with the onset of shock stall. The results suggest that delta wing configurations might also be susceptible to the same type of instability.

2. With one possible exception, stall flutter was not observed over the Mach number and angle-of-attack ranges investigated.

3. Conditions of maximum buffet intensity occurred at angles of attack ranging from 10° to 14°. Quantitative results for the peak dynamic bending moments due to buffet are given in a form suitable for predicting full scale loads.

Ames Research Center
National Aeronautics and Space Administration
Moffett Field, Calif. 94035, August 27, 1973

REFERENCES

1. Surber, T. E.; Bornemann, W. E.; and Miller, W. D.: Wing Optimization for Space Shuttle Orbiter Vehicles. Space Shuttle Aerothermodynamics Technology Conference. Volume III - Aerodynamics. NASA TM X-2508, 1972, pp. 831–859.

2. Erickson, Larry L.; Gambucci, Bruno J.; and Wilcox, Phillip R.: Effects of Space Shuttle Configurations on Wing Buffet and Flutter. Part II, Thick High-Aspect-Ratio Wing. NASA Space Shuttle Technology Conference. Volume III - Dynamics & Aeroelasticity. NASA TM X-2274, 1971, pp. 201–229.

3. Bisplinghoff, Raymond L.; Ashley, Holt; and Halfman, Robert L.: Aeroelasticity. Addison-Wesley Publishing Company, Inc., 1955, Cambridge, Mass.

4. Cole, Henry A., Jr.: On-The-Line Analysis of Random Vibrations. AIAA Paper No. 68-288, AIAA/ASME 9th Structures, Structural Dynamics and Materials Conference, Palm Springs, Calif., April 1-3, 1968.

5. Jacobsen, Lydik S.; and Ayre, Robert S.: Engineering Vibrations, With Applications to Structures and Machinery. McGraw-Hill Book Company, Inc., 1958, pp. 335–339.

6. Runyan, Harry L.; Cunningham, Herbert J.; and Watkins, Charles E.: Theoretical Investigation of Several Types of Single Degree of Freedom Flutter. J. Aeron. Sci., vol. 19, no. 2, Feb. 1952, pp. 101–110, 126.

7. Erickson, Albert L.; and Stephenson, Jack D.: A Suggested Method of Analyzing for Transonic Flutter of Control Surfaces Based on Available Experimental Evidence. NACA RM A7F30, 1947.

8. Rainey, A. Gerald: Preliminary Study of Some Factors Which Affect the Stall-Flutter Characteristics of Thin Wings. NACA TN 3622, 1956.

9. Robinson, Robert C.; Wilcox, Phillip R.; Gambucci, Bruno J.; and George, Robert E.: Dynamic Response of a Family of Axisymmetric Hammerhead Models to Unsteady Aerodynamic Loading. NASA TN D-4504, 1968.

10. Jones, Robert T.; and Cohen, Doris: Aerodynamics of Wings at High Speeds. Aerodynamic Components of Aircraft at High Speeds, Vol. VII of High Speed Aerodynamics and Jet Propulsion. Allen F. Donovan, and H. R. Lawrence, eds. Princeton University Press, 1957, pp. 34–35.

11. Feldman, Fritz K.: Untersuchung von Symmetrischen Tragflügelprofilen bei hohen Unterschallgeschwindigkeiten in einem geschlossenen Windkanal. Mitt. 14, Inst. für Aerodynamik. A. G. Gebr. Leeman and Co., Zürich, 1948.

12. Liepmann, Hans Wolfgang: The Interaction between Boundary Layer and Shock Waves in Transonic Flow. J. Aeron. Sci., vol. 13, no. 12, Dec. 1946, pp. 623–637.

13. Loving, Donald L.: Wind-Tunnel-Flight Correlation of Shock-Induced Separated Flow. NASA TN D-3580, 1966.

14. Cahill, Jones, F.; and Cooper, Bill L.: Flight Test Investigation of Transonic Shock-Boundary Layer Phenomena. AFFDL-TR-68-84, Vol. 1, Lockheed-Georgia Co., 1968.

15. Becker, John V.: Characteristics of Wing Sections at Transonic Speeds. NACA - University Conference on Aerodynamics, held at Langley Aeronautical Laboratory, Langley Field, Va., June 21-23, 1948, pp. 127–150.

16. Rainey, A. Gerald: Some Observations on Stall Flutter and Buffeting. NACA RM L53E15, 1953.

17. Mead, D. J.: Linear Dynamical Systems Under Random Loading. Noise and Acoustic Fatigue in Aeronautics. E. J. Richards and D. J. Mead, eds. John Wiley & Sons, Ltd., New York, 1968, pp. 315.

18. Jones, J. G.: The Dynamic Analysis of Buffeting and Related Phenomena. RAE Tech. Memo Aero 1401, 1972.

19. Doggett, Robert V., Jr.; and Hanson, Perry W.: An Aeroelastic Model Approach for the Prediction of Buffet Bending Loads on Launch Vehicles. NASA TN D-2022, 1963.

20. Rainey, A. Gerald: Measurement of Aerodynamic Forces for Various Mean Angles of Attack on an Airfoil Oscillating in Pitch and on Two Finite-Span Wings Oscillating in Bending with Emphasis on Damping in the Stall. NACA Rept. 1305, 1957.

21. Crandall, Stephen H.; and Mark, William D.: Random Vibration in Mechanical Systems. Academic Press, 1963, pp. 44–48.